SEMI-ANALYTICAL ADAPTIVE GUIDANCE ALGORITHM FOR FAST RETARGETING MANEUVERS COMPUTATION DURING PLANETARY DESCENT AND LANDING

Paolo Lunghi, Michéle Lavagna, and Roberto Armellin

Politecnico di Milano, Department of Aerospace Science and Technology (DAST), Via La Masa 34, 20156 Milano-Italy

ABSTRACT

This work focuses on an adaptive guidance algorithm for planetary landing that updates the trajectory to the surface by means of a minimum fuel optimal control problem solving. A semi-analytical approach is proposed. The trajectory is expressed in a polynomial form of minimum order to satisfy a set of boundary constraints derived from initial and final states and attitude requirements. By imposing boundary conditions, a fully determined guidance profile is obtained, function of only two parameters: time-of-flight and initial thrust magnitude. The optimal guidance computation is reduced to the determination of these parameters, according to additional path constraints due to the actual lander architecture: available thrust and control torques, visibility of the landing site, and other additional constraint not implicitly satisfied by the polynomial formulation. Solution is achieved with a simple two-stage compass search algorithm: the algorithm firstly finds a feasible solution; whenever detected, it keeps solving for the optimum; nonlinear constraints are evaluated numerically, by pseudospectral methods. Results on different scenarios for a Moon landing mission are shown and discussed to highlight the effectiveness of the proposed algorithm and its sensitivity to the navigation errors.

Key words: pinpoint landing; adaptive guidance; retargeting; hazard avoidance.

1. INTRODUCTION

An autonomous, precise and safe landing capability is a key feature for the next space systems generation. The chance to adapt and correct the final landing pinpoint almost up to the touch down increases both the robustness and the flexibility of the vehicle operations: surface hazards can be safely avoided, unpredictable events such failures can be managed and in loco detected scientifically relevant places may be approached, slightly changing the landing trajectory, being already nearby the final target. One of the big challenges to deal with, in such a scenario, is represented by the short duration of the terminal descent phase together with the telecommunications delay because of the interplanetary distances: they clearly asks for a high level of on board autonomy in the Guidance Navigation and Control during this phase, coupled with light and fast computational mechanisms.

A trajectory based on a quartic polynomial in time was used during the Apollo missions [6]. A derivative of the Apollo lunar descent guidance was still considered in recent years, for the Mars Science Laboratory (MSL) [12]. Various other approaches to obtain both numerical and approximate solutions of the pinpoint landing terminal guidance problem have been described over the last few years. In [10] the first-order necessary conditions for the problem are developed, and it is shown that the optimal thrust profile has a maximum-minimum-maximum structure. Direct numerical methods for trajectory optimization have been widely investigated, not requiring the explicit consideration of the necessary conditions [2]. These methods have been used together with Chebyshev pseudospectral techniques, in order to reduce the number of the optimization variables [3]. Also convex programming approach has been proposed, in order to guarantee the convergence of the optimization [1]. Direct collocation methods has showed that the size of the region of feasible initial states, for which there exist feasible trajectories, can be increased drastically (more than twice) compared to the traditional polynomial-based guidance approaches, but at the price of a higher computational cost [1].

In this paper a guidance algorithm capable to dynamically recompute and correct the landing trajectory during the descent is developed, allowing the on-board choice of the landing site, required by systems that have to operate in full autonomy. A semi-analytical approach is proposed, in order to conjugate the low computational cost of polynomial approximation to the larger flexibility of direct optimization methods. Fuel consumption has been used as optimality criterion.

2. THE GUIDANCE ALGORITHM

The retargeting problem, as part of an hazard detection and avoidance system, involves only the last part of the landing. Distances, for both downrange and altitude, are small (less than 3 km) compared to the planet's radius and the assumption of a constant gravity field with flat ground

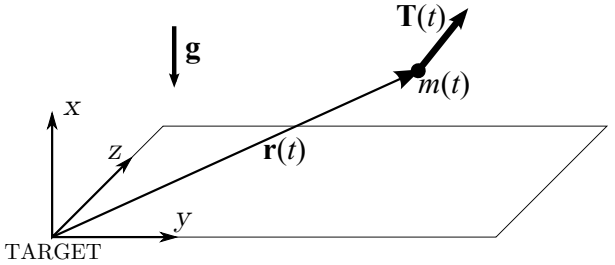

Figure 1: Ground Reference System.

is appropriate.
No aerodynamic forces are considered. The eventual presence of atmosphere (especially with low density, as in the case of Mars) could be however negligible, due to the relative low velocity involved (on the order of $100\,\mathrm{m\,s^{-1}}$), and these forces can be treated as disturbances [1].

The translational dynamics of the spacecraft, expressed in a *Ground reference system* (Fig. 1), are described by the equations:

$$\begin{cases} \ddot{\mathbf{r}}(t) = \dfrac{\mathbf{T}(t)}{m(t)} + \mathbf{g}, \\ \dot{m}(t) = -\dfrac{T(t)}{I_{\mathrm{sp}} g_0}, \end{cases} \tag{1}$$

where $\mathbf{r} \in \mathbb{R}^3$ is the position vector, $\mathbf{T} \in \mathbb{R}^3$ is the thrust vector, m is the mass of the spacecraft, $\mathbf{g} \in \mathbb{R}^3$ is the constant gravity field of the planet, I_{sp} the specific impulse of the main engine and g_0 the standard gravity acceleration on Earth. $T = \|\mathbf{T}\|$ is the net thrust magnitude.

The main thruster is assumed to be rigidly connected

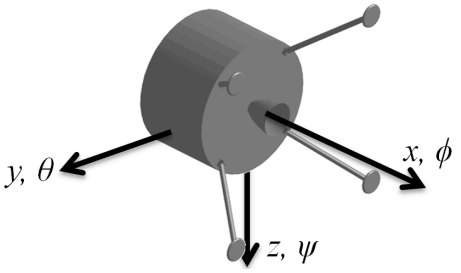

Figure 2: Body-fixed Reference System.

to the spacecraft, so the direction of the thrust vector is determined directly by the spacecraft attitude, expressed in Euler angles, $\{\phi, \theta, \psi\}^T$, in the 231 form. ϕ is the *Roll* angle, θ is the *Pitch* angle and ψ is the *Yaw* angle (Fig. 2). The 231 form is preferred to the more traditional 321, because allows to avoid the presence of singularities in the angles determination, in the field of application of the landing phase. The thrust vector can be represented as:

$$\mathbf{T}(t) = -T(t) \begin{bmatrix} \cos\psi(t) \sin\theta(t) \\ \cos\psi(t) \cos\theta(t) \\ -\sin\psi(t) \end{bmatrix}. \tag{2}$$

At the time instant t_0 in which a retargeting is commanded, position and speed of the spacecraft are known. The initial acceleration depends on the initial thrust magnitude T_0, from Eqns. (1) and (2). At the end of the maneuver, at time t_{f}, target position and speed are required. Also, the spacecraft is desired to have a vertical attitude. This implies that the horizontal components of the thrust vector must be zero:

$$\ddot{r}_{\mathrm{y}}(t_{\mathrm{f}}) = \ddot{r}_{\mathrm{z}}(t_{\mathrm{f}}) = 0. \tag{3}$$

Then, a total of 17 boundary constraints are available. The three components of the acceleration can be expressed in a polynomial form. The minimum order needed to satisfy boundary constraints is 2 for the vertical axis, 3 for the horizontal components:

$$\ddot{r}_{\mathrm{x}}(t) = \ddot{r}_{\mathrm{x}}(t_0) + C_{1\mathrm{x}} t + C_{2\mathrm{x}} t^2, \tag{4}$$

$$\ddot{r}_{\mathrm{y/z}}(t) = \ddot{r}_{\mathrm{y/z}}(t_0) + C_{1\mathrm{y/z}} t + C_{2\mathrm{y/z}} t^2 + C_{3\mathrm{y/z}} t^3. \tag{5}$$

Integrating the acceleration two times, and applying boundary constraints, the trajectory is completely defined, function of t_{f} and T_0.
From the acceleration profile, the thrust-to-mass ratio $\mathbf{P}(t)$, and then the thrust vector, can be obtained:

$$\mathbf{P} = \mathbf{T}/m = \ddot{\mathbf{r}} - \mathbf{g} \quad \Rightarrow \quad \mathbf{T} = m\mathbf{P}. \tag{6}$$

The mass versus time trend is determined by a first order linear ordinary differential equation whose solution is:

$$m(t) = m_0 \exp\left(-\int_{t_0}^{t_{\mathrm{f}}} \frac{\|\mathbf{P}(t)\|}{I_{\mathrm{sp}} g_0} dt \right). \tag{7}$$

The analytical calculation of the integral exponent is complex, but it can be easily obtained trough numerical integration, using Chebyshev pseudospectral methods, such as the Clenshaw-Curtis quadrature [11].
From the thrust unit vector $\hat{\mathbf{n}} = \mathbf{T}/\|\mathbf{T}\|$ a complete guidance profile, in terms of Euler angles and thrust magnitude, is obtained, function of initial thrust magnitude T_0 and time-of-flight $t_{\mathrm{ToF}} = t_{\mathrm{f}} - t_0$:

$$\theta = \tan^{-1}\left(\hat{n}_x / \hat{n}_y\right), \; -\pi \leq \theta \leq 0, \tag{8}$$

$$\psi = \tan^{-1}\left(\hat{n}_z \left(\hat{n}_x^2 + \hat{n}_y^2\right)^{-0.5}\right), \; -\frac{\pi}{2} \leq \psi \leq \frac{\pi}{2}, \tag{9}$$

$$\phi = 0. \tag{10}$$

2.1. Additional Constraints

The problem is so reduced to find the values of T_0 and t_{ToF}, according to any additional constraint not implicitly satisfied by the polynomial formulation, in order to minimize the fuel consumption. Assuming $\mathbf{x} = \{t_{\mathrm{ToF}}, T_0\}^T$, the cost function is $f(\mathbf{x}) = m(t_0) - m(t_{\mathrm{f}})$, and the problem can be expressed in the form:

$$\min_{\mathbf{x}} f(\mathbf{x}) \text{ such that } \begin{cases} \mathbf{x}_L \leq \mathbf{x} \leq \mathbf{x}_U \\ \mathbf{c}_L \leq \mathbf{c}(\mathbf{x}) \leq \mathbf{c}_U \end{cases}. \tag{11}$$

The optimization variables $\mathbf{x}$ are not allowed to take any value, but they have a finite domain with lower bound

$\mathbf{x}_L$ and upper bound $\mathbf{x}_U$. These are called *box constraints*. The elements of $\mathbf{c}(\mathbf{x})$ are generally non-linear functions of the optimization variables, also bounded between lower and upper limits $\mathbf{c}_L$ and $\mathbf{c}_U$. These constraints need to be satisfied during all the landing maneuver, so they are called *path constraints*. Finally, the polynomial formulation does not explicitly consider boundary constraint on mass. This implies the additional constraint:

$$m_{\text{dry}} \leq m(t_{\text{f}}) \leq m_0. \tag{12}$$

Box Constraints
The thrust magnitude is bounded to the thrust available on-board:

$$0 < T_{\text{min}} \leq T_0 \leq T_{\text{max}}. \tag{13}$$

The time-of-flight must be greater than zero, while its theoretical upper limit is determined by the maximum amount of fuel on board m_{fuel}.

$$0 \leq t_{\text{ToF}} \leq t_{\text{max}} = m_{\text{fuel}} \frac{I_{\text{sp}} g_0}{T_{\text{min}}}. \tag{14}$$

Path Constraints
During the landing the required thrust magnitude cannot exceed the limit imposed by the actual engine on board:

$$T_{\text{min}} \leq T(t) \leq T_{\text{max}}. \tag{15}$$

Euler angles rate of change is subject to the actual control torques M_{Cmax} available by the ACS. The extrapolation of the exact torques from angles is not immediate, due to coupled terms in the attitude dynamics. The objective is to characterize such a rotational rate constraint without coupling the problem to the rotational dynamics, in order to save computation time. Torques are approximated by the decoupled term due to the angular acceleration. This corresponds to the reality in case of small angles and low angular speed, a condition not at all verified during a retargeting, and it can be used only for an estimate:

$$-\rho M_{C\text{max}} \leq I_{\text{max}} \ddot{\theta}(t) \leq \rho M_{C\text{max}}, \tag{16}$$

$$-\rho M_{C\text{max}} \leq I_{\text{max}} \ddot{\psi}(t) \leq \rho M_{C\text{max}}. \tag{17}$$

I_{max} is the maximum moment of inertia at initial time t_0. This allows to avoid the on-board calculation of inertia properties, and gives a margin of safety in the torques calculation. An additional margin of safety $0 < \rho < 1$ can be applied.
In a feasible landing path altitude is always greater than zero. This constraint can be improved considering a *glide-slope constraint*. In this case the lander is required to remain in a cone defined by the minimum slope angle γ_{max}, as showed in Fig. 3. This constraint has a dual purpose: it assures that the the lander does not penetrate the ground, even in presence of bulky terrain features near the landing site; at the same time it limits the angle of view onto the target. In fact, the performances of vision-based navigation systems depend on inclination between the trajectory and the ground [4, 9]. The constraint take the form:

$$-\infty \leq \|\mathrm{S}\mathbf{r}(t)\| + \mathbf{c}^T \mathbf{r}(t) \leq 0, \tag{18}$$

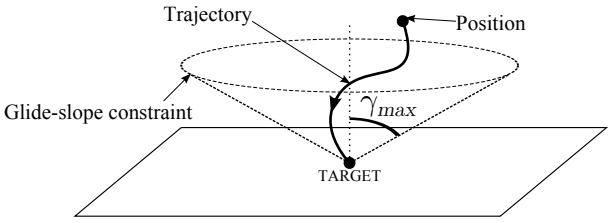

Figure 3: Glide-slope constraint.

where

$$\mathrm{S} = \begin{bmatrix} 0 & 1 & 0 \\ 0 & 0 & 1 \end{bmatrix}, \tag{19}$$

$$\mathbf{c}^T = [-\tan\gamma_{\text{max}} \quad 0 \quad 0]. \tag{20}$$

Path constraints need to be satisfied at every time instant during the landing. Pseudospectral techniques allow to evaluate them discretely. Derivative terms are obtained by the use of the Chebyshev differentiation matrix.

2.2. Optimization Algorithm

The optimization problem (11) is solved through a modified version of the *compass search method*, enhanced in order to handle also non-linear constraints. First, the optimization variables are normalized, in order to give them the same relative weight in the optimization:

$$\tilde{\mathbf{x}} = \frac{\mathbf{x} - \mathbf{x}_L}{\mathbf{x}_U - \mathbf{x}_L} \quad \Leftrightarrow \quad \mathbf{x} = \tilde{\mathbf{x}}(\mathbf{x}_U - \mathbf{x}_L) + \mathbf{x}_L. \tag{21}$$

Normalized optimization variables can vary between 0 and 1. Then, a feasibility function $F(\tilde{\mathbf{x}})$ is created, defined as:

$$F(\tilde{\mathbf{x}}) = \sum_{j=0}^{N_C} \frac{1}{w_{\text{F}j}} \max(0, \tilde{c}_j), \tag{22}$$

where $\tilde{c}_j$ are the components of a generalized constraints vector $\tilde{\mathbf{c}}(\tilde{\mathbf{x}})$, and w_{F} is a vector of weights, in order to normalize different constraints that can have different orders of magnitude:

$$\tilde{\mathbf{c}}(\tilde{\mathbf{x}}) = \begin{bmatrix} \mathbf{c}_L - \mathbf{c}(\tilde{\mathbf{x}}) \\ \mathbf{c}(\tilde{\mathbf{x}}) - \mathbf{c}_U \\ 0 - \tilde{\mathbf{x}} \\ \tilde{\mathbf{x}} - 1 \end{bmatrix}, \quad \mathbf{w}_{\text{F}} = \begin{bmatrix} \mathbf{c}_U - \mathbf{c}_L \\ \mathbf{c}_U - \mathbf{c}_L \\ \mathbf{x}_U - \mathbf{x}_L \\ \mathbf{x}_U - \mathbf{x}_L \end{bmatrix}. \tag{23}$$

A feasible set of optimization variables $\tilde{\mathbf{x}}$ corresponds to a null value of the feasibility function. On the contrary, in case of infeasibility $F(\tilde{\mathbf{x}}) > 0$. The optimization algorithm operates in two phases. Firstly, an unconstrained compass search on the function $F(\tilde{\mathbf{x}})$ is performed. The search is stopped when a feasible point is found ($F(\tilde{\mathbf{x}}) = 0$), or when the iteration limit is reached. In this case, the problem is classified as infeasible.
If the fist step is successful the algorithm keeps solving for the optimum through an unconstrained search on the modified cost function $\Phi(\tilde{\mathbf{x}})$, defined as:

$$\Phi(\tilde{\mathbf{x}}) = f(\tilde{\mathbf{x}}) + \eta \operatorname{sgn}\big(F(\tilde{\mathbf{x}})\big), \tag{24}$$

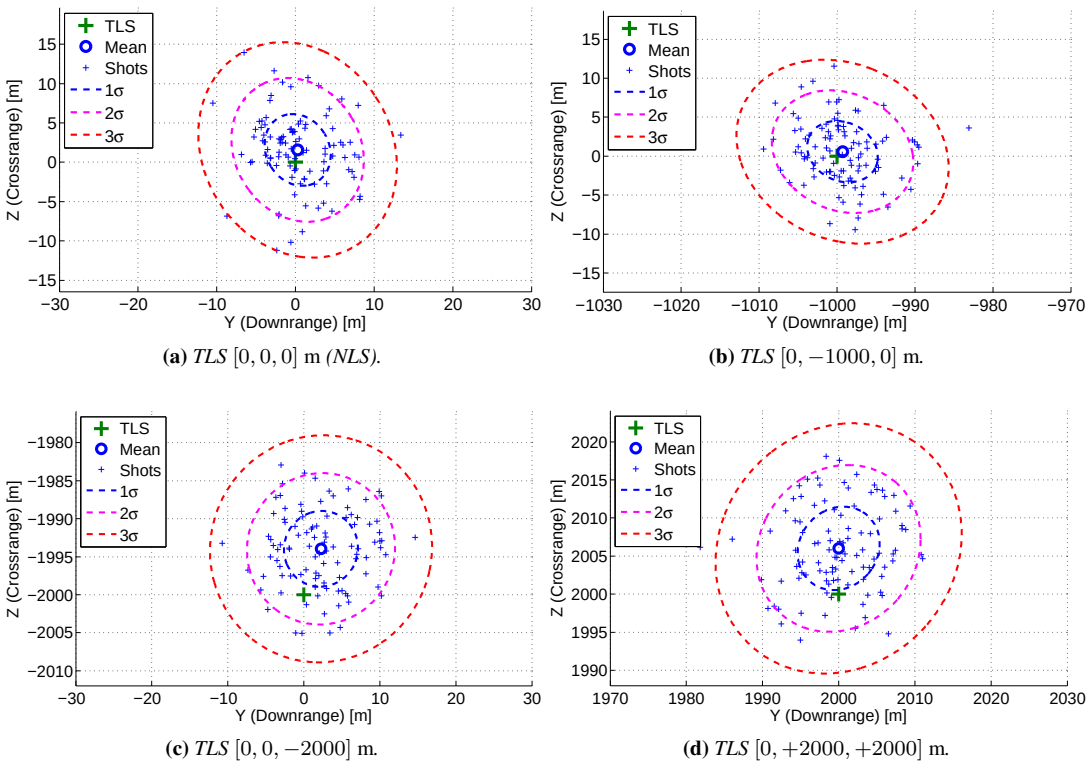

(a) *TLS* $[0, 0, 0]$ m *(NLS).*

(b) *TLS* $[0, -1000, 0]$ m.

(c) *TLS* $[0, 0, -2000]$ m.

(d) *TLS* $[0, +2000, +2000]$ m.

Figure 4: Landing Position Sensitivity to TLS coordinates. Initial dispersion ± 25 m, $\pm 0.4\,\mathrm{m\,s^{-1}}$ (1σ).

where $f(\tilde{\mathbf{x}})$ is the original cost function of the problem (11), and $\eta = 10^{100}$, a number certainly greater than the maximum value that cost function can assume.

3. LANDING SIMULATION

The guidance algorithm has been tested through a 6DoF retargeting simulator of a lunar landing, realized in Matlab® and Simulink® environment. The ESA Lunar Lander mission has been taken as reference scenario [8]. Assumptions on lander architecture are summarized in Tab. 1.

Table 1: Lander architecture assumptions.

Feature	Value
Mass @ 2000 m altitude	865 kg
Dry mass m_{dry}	790 kg
I_{sp}	325 s
I_{max}	1000 kg m^2
T_{min}	1000 N
T_{max}	2320 N
$M_{C\mathrm{max}}$	40 N m

The simulation starts at 2000 m altitude on a nominal landing trajectory. A vertical terminal descent phase is supposed to be after the retargeting. Then, target states for the guidance algorithm are $\mathbf{r}(t_{\mathrm{f}}) = \{30, 0, 0\}$ m and $\dot{\mathbf{r}}(t_{\mathrm{f}}) = \{-1.5, 0, 0\}\,\mathrm{m\,s^{-1}}$. A disturbance torque is introduced by thrust misalignment from the spacecraft center of mass. Errors in the states passed to the guidance block are introduced in order to emulate a navigation system. Attitude is supposed to be estimated by an Inertial Measurement Unit (IMU), whose performances are summarized in Tab. 2.

The presence of a vision-based navigation system is assumed in order to estimate position and speed. This kind of systems makes use of a radar or laser altimeter to estimate the altitude with which the images taken by cameras are resized to the proper scale. Since altimeters absolute error increases with the distance from the ground, the error in the estimate is modeled as a Gaussian random error with zero mean and standard deviation varying linearly with the altitude.

Table 2: IMU performance properties.

Property	Value	UoM
Scale factor	1	ppm
Misalignment Error	170	µrad
Bias Error	0.005	deg/h
ARW noise density	0.005	deg/$\sqrt{\mathrm{h}}$

The guidance subsystem recalculates the trajectory whenever a retargeting is commanded and anyway every 5 s, in order to cope with measure dispersions. From the guid-

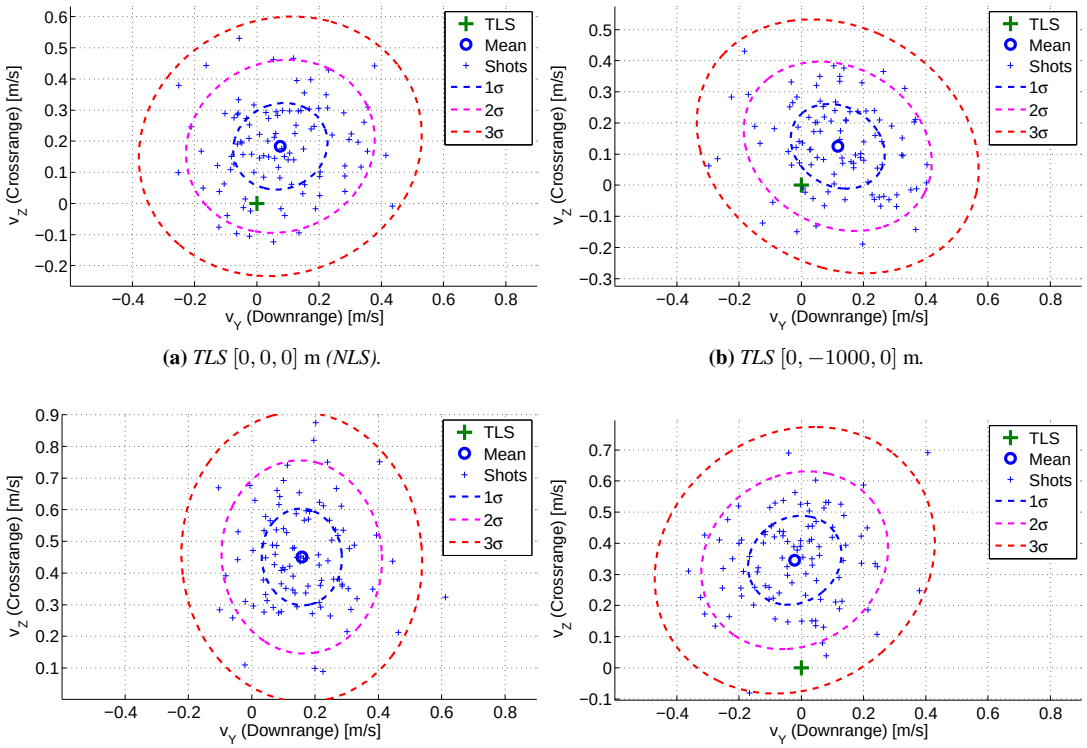

(a) *TLS* $[0, 0, 0]$ m *(NLS).*

(b) *TLS* $[0, -1000, 0]$ m.

(c) *TLS* $[0, 0, -2000]$ m.

(d) *TLS* $[0, 2000, 2000]$ m.

Figure 5: Landing Velocity Sensitivity to the Target Landing Site coordinates. Initial dispersion ± 25 m, $\pm 0.4\,\mathrm{m\,s^{-1}}$ (1σ).

ance profile, at every update of the control system, target quaternions and angular velocities are computed, and exploited by a PID controller to calculate theoretical control torques. The attitude is assumed to be actually controlled by a cluster of chemical thrusters capable to supply a constant torque of $\pm 40\,\mathrm{N\,m}$ on every axis. So theoretical control torques are processed by a PWPF modulator that commands thrusters firings.
The considered guidance and control systems update rate is 20 Hz.

3.1. Sensitivity to Landing Site

Monte Carlo simulations have been run to verify the sensitivity of the system with respect to the Target Landing Site (TLS) coordinates. Every simulation considers 100 samples affected by navigation errors; the assumed error is 25 m (1σ) and $0.4\,\mathrm{m\,s^{-1}}$ (1σ) at 2000 m altitude, respectively for position and speed along all axes, linearly decreasing with altitude. Diversions up to ± 2000 m along both the horizontal directions from Nominal Landing Site (NLS) have been considered. Four representative cases of diversion are presented:

(a) TLS $\{0, 0, 0\}^T$ m (retargeting on NLS);

(b) TLS $\{0, -1000, 0\}^T$ m (Downrange brake);

(c) TLS $\{0, 0, -2000\}^T$ m (Crossrange diversion);

(d) TLS $\{0, +2000, +2000\}^T$ m (max distance tested).

The obtained results are shown in Fig. 4 for the position and in Fig. 5 for the speed. The landing precision appears to be independent by the magnitude of the requested diversion.

3.2. Sensitivity to Navigation Errors

Monte Carlo simulations have been exploited to verify the sensitivity of the system to the initial navigation dispersion. Each simulation considers 100 samples. The same targeting scenario is considered for all the simulations, with the TLS collocated at $[0, +1000, +1000]$ m from the Nominal Landing Site. Each simulation has a different value of initial error standard deviation in the determination of position. Standard deviation (STD) values of 45, 25 and 10 m has been considered. Also a simulation without navigation errors has been performed, in order to determinate the impact of the navigation dispersion relatively to the accuracy obtained only from the control. In all the simulations the initial velocity error STD is assumed constant at $0.4\,\mathrm{m\,s^{-1}}$.
Performances obtained are shown in Fig. 6 and in Fig. 7, respectively for position and speed. Dispersion due to control is at least one order of magnitude lower than the one due to navigation. This proves that landing precision is mainly affected by navigation errors.

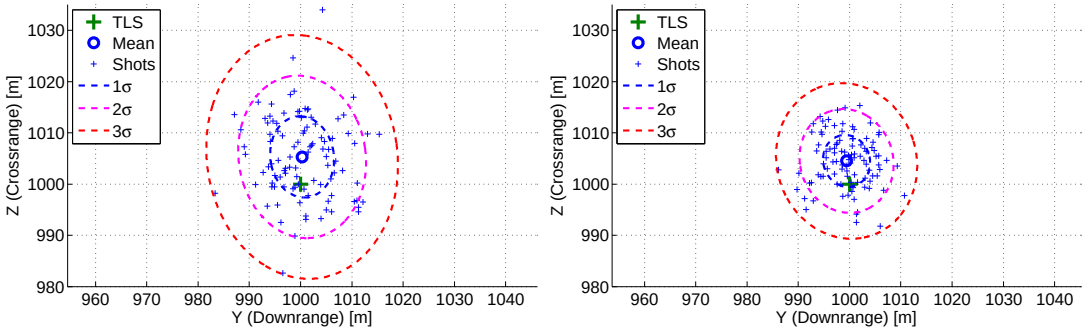

(a) *Error STD* 45 m *(1σ).*

(b) *Error STD* 25 m *(1σ).*

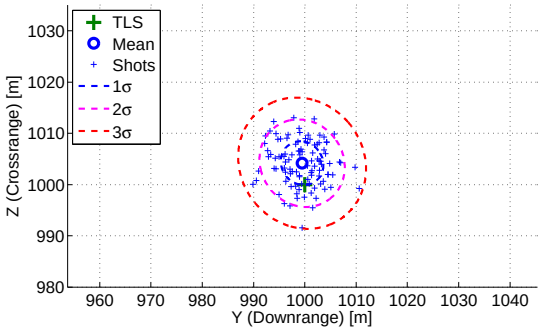

(c) *Error STD* 10 m *(1σ).*

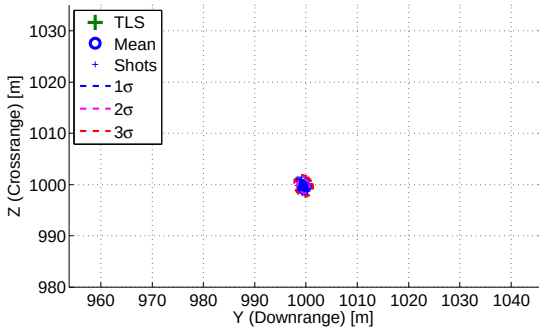

(d) *Exact measures.*

Figure 6: Position Sensitivity to initial Navigation errors. TLS $[0, +1000, +1000]$.

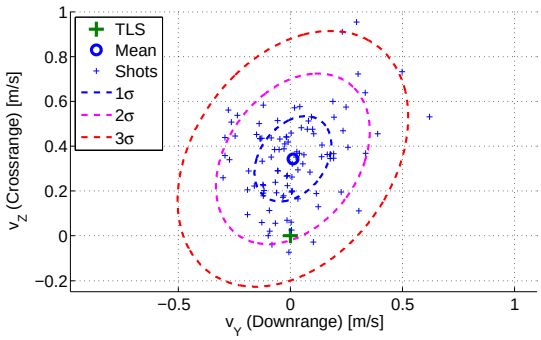

(a) *Error STD* 45 m *(1σ).*

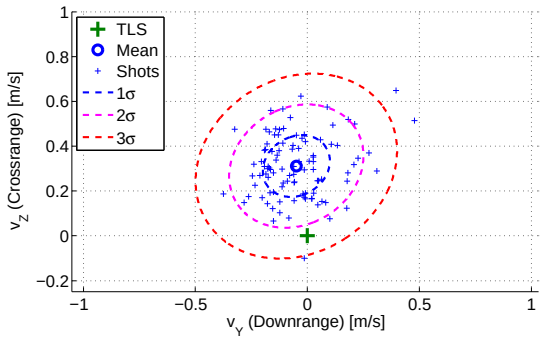

(b) *Error STD* 25 m *(1σ).*

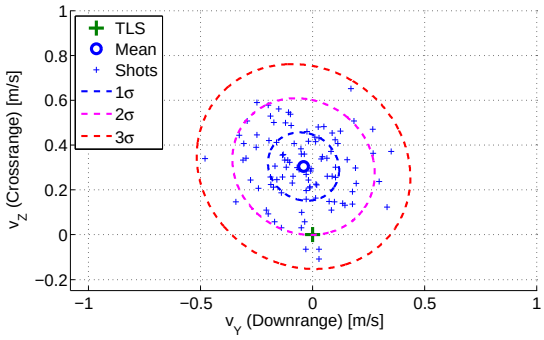

(c) *Error STD* 10 m *(1σ).*

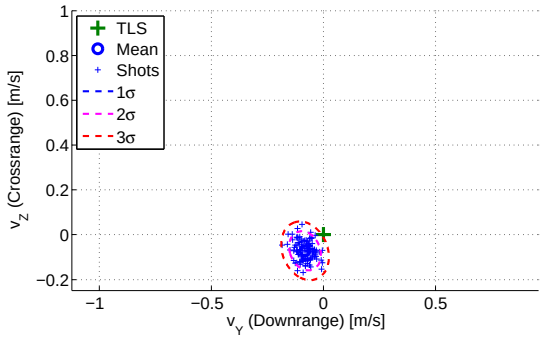

(d) *Exact measures.*

Figure 7: Landing Velocity Sensitivity to Navigation dispersions. TLS $[0, +1000, +1000]$.

3.3. Camera Field of View

A preliminary study on cameras Field of View (FoV) for navigation and/or hazard detection has been performed. The smooth attitude profile imposed by the trajectory polynomial approximation guarantees the absence of sudden maneuvers, allowing a continuous landmarks tracking. A single camera, pointing towards the roll axis has been assumed. By way of example, Fig. 8 shows how the intersection between the camera line of sight and the ground varies during a representative retargeting, of $[0, +750, -1200]$ m. The camera pointing depicted into the graph is taken every 0.5 s, an update rate lower than the actual camera frame rate, that is considered between 10 and 20 Hz [4]. Tracked landmarks pass into the FoV in a continuous way, allowing relative navigation.

The nominal landing trajectory is designed in order to

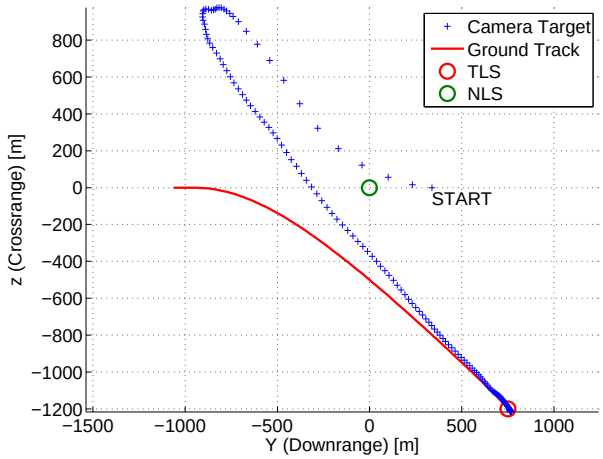

Figure 8: Camera pointing during retargeting.

have the necessary time for hazard mapping before the first retargeting. But if a second retargeting is required, during the first maneuver the TLS is required to be in sight for the time necessary to update the hazard map. Since the FoV angle considered is between 50 and 70° [4], the LS visibility can be considered lost when the angle between the line of sight and the TLS direction is greater than 25-35°, depending by the actual HDA system architecture.

Fig. 9 shows the trend of this angle during the same maneuver of Fig. 8, and for other two retargetings: a minor diversion of $[0, +150, +150]$ m and a large retargeting of $[0, +1700, +1600]$ m. It can be seen that the oscillatory movement implied by the maneuver might cause this loss just after the diversion start. However, the visibility is recovered at lower altitudes, enabling the recreation of the hazard map. This behaviour is obtained in all the analysed cases. For minor retargetings, the oscillation magnitude is smaller, and the LS visibility can be maintained along the maneuver. Diversions up to ± 2000 m on both the horizontal axes have been tested. In diversions above 1500 m, greater oscillations are counterbalanced by greater time-of-flight, that guarantees more time for a second retargeting.

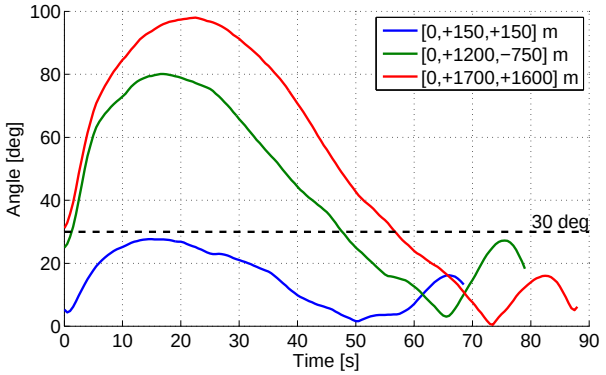

Figure 9: TLS-Sightline angle on different Target Landing Sites.

If a double retargeting is expected, a change in the retargeting strategy, in order to guarantee the necessary visibility, could be considered. One possibility is a two-step retargeting similar to that suggested in [5]: the first diversion is commanded at high altitude (2000 m or above if it is possible), pointing towards the vertical onto selected TLS at an intermediate altitude (400-600 m). In this way the system is able to perform, at the end of this maneuver, a short vertical descent at constant speed, during which the hazard map can be updated with more resolution. Then, if requested, a second diversion until the terminal descent phase and the touchdown can be commanded. If not needed, the descent can be completed with a fuel optimal vertical descent, whose solution is known in close form [7].

Another possible choice is a modification in the hazard detection system architecture, such as the use of multiple cameras, or the use of gimbals, in order to increase the Field of View [9].

4. CONCLUSIONS

The purpose of this work was the development of a retargeting algorithm for planetary landing, capable of updating and correcting a landing trajectory almost to the touchdown. A classical polynomial approach has been extended, in order to improve flexibility in the landing site choice, and to consider additional non linear constraints during the descent. The resulting algorithm has light computational weight, and maintains a high divert capability even with the use of a basic optimization algorithm such as compass search.

The functionality and the robustness of the algorithm have been tested by applying it in a simulation of a complete retargeting. The guidance scheme has been coupled with an attitude controller, and perturbed states have been exploited in order to emulate navigation system errors. In order to identify possible sources of errors in placing the spacecraft on target, a dispersion analysis has been performed, and it has been observed that navigation errors play a major role in determining the accuracy at touchdown.

REFERENCES

[1] Acikmeşe, B. and Ploen, S. R. (2007). Convex programming approach to powered descent guidance for Mars landing. *Journal of Guidance, Control and Dynamics*, 30(5).

[2] Betts, J. T. (1998). Survey of numerical methods for trajectory optimization. *Journal of Guidance, Control, and Dynamics*, 21(2):193–207.

[3] Fahroo, F. and Ross, I. M. (2002). Direct trajectory optimization by a Chebyshev pseudospectral method. *Journal of Guidance, Control and Dynamics*, 25(1).

[4] Flandin, G., Polle, B., Despré, N., Lheritier, J., Perrimon, N., and Blanc-Paques, P. (2010). Maturing vision based navigation solutions to space exploration. In *AIAA Guidance, Navigation, and Control Conference*. American Institute of Aeronautics and Astronautics.

[5] Johnson, M. (2006). A parameterized approach to the design of lunar lander attitude controllers. In *AIAA Guidance, Navigation, and Control Conference and Exhibit*. American Institute of Aeronautics and Astronautics.

[6] Klumpp, A. R. (1974). Apollo lunar descent guidance. *Automatica*, 10(2):133–146.

[7] Meditch, J. (1964). On the problem of optimal thrust programming for a lunar soft landing. *Automatic Control, IEEE Transactions on*, 9(4):477–484.

[8] Pradier, A., Gardini, B., Rosa, D., Fisackerly, R., Carpenter, J., Houdou, B., and Philippe, C. (2011). The ESA lunar lander mission. In *AIAA SPACE 2011 Conference & Exposition*. American Institute of Aeronautics and Astronautics.

[9] Riedel, J., Vaughan, A., Werner, R. A., Tseng-Chan, W., Nolet, S., Myers, D., Mastrodemos, N., Lee, A., Grasso, C., Ely, T., and Bayard, D. (2010). Optical navigation plan and strategy for the lunar lander Altair; OpNav for lunar and other crewed and robotic exploration applications. In *AIAA Guidance, Navigation, and Control Conference*. American Institute of Aeronautics and Astronautics.

[10] Topcu, U., Casoliva, J., and Mease, K. (2005). Fuel efficient powered descent guidance for Mars landing. In *AIAA Guidance, Navigation, and Control Conference and Exhibit*. American Institute of Aeronautics and Astronautics.

[11] Trefethen, L. N. (2000). *Spectral methods in Matlab*. Society for Industrial and Applied Mathematics.

[12] Wong, E., Masciarelli, J., and Singh, G. (2002). Autonomous guidance and control design for hazard avoidance and safe landing on Mars. In *AIAA Atmospheric Flight Mechanics Conference and Exhibit*. American Institute of Aeronautics and Astronautics.